Energy 167 (2019), pp. 211-223.

Improved mixture quality by advanced dual-nozzle, included-angle split injection in HSDI engine: Exergetic exploration

*Hadi Taghavifar[a,] , Arash Nemati[b *], F.J. Salvador[c], J. de la Morena[c]*

[a]Department of Mechanical Engineering, Faculty of Engineering, Malayer University, Iran.

[b]Faculty of Mechanical Engineering, University of Tabriz, 29th Bahman Blvd, Tabriz, Iran

Corresponding author.

[c]CMT-Motores Térmicos, Universitat Politècnica de València.

Abstract

A Ford 1.8 l high speed diesel engine (HSDI) is utilized for a thorough investigation on split dual injection with two included-angle nozzles. The system is equipped with variable-geometry turbocharging (VGT) and high-pressure common-rail (HPCR) technologies which lets multi-injections per cycle. The share of fuel between pulses is divided in three portions of 70-30, 80-20, and 90-10 with included angles of 10, 20, and 30 while the dwell time between pulses are 5CA, 10CA, 15CA, and 20CA. The results demonstrate that the optimum option is 70 (5) 30-30deg with the best homogeneity of mixture (UI = 0.9742) and peak temperature (T_{max} = 2011.58 K) that yield maximum thermo-mechanical exergy amounting to 439 J. In addition, the highest amount of accumulative irreversibility happens for 90 (10) 10-20deg. It is found that there is a relation between mixture uniformity and accumulative work/heat exergy, whereas high rate of pressure rise (RPR) contribute to irreversibility rate or exergy destruction in diesel engine, i.e. RPR (80-20) = 904.67 kPa/deg. More, the results are in agreement with literature reporting that higher in-cylinder temperature (T_{max} (70 (5) 30-30deg) = 2011.58 K)) can possibly decrease the accumulative irreversibility (147.9 J).

Keywords: Diverged included spray; Exergy; Irreversibility; Split injection; Uniformity index

1. Introduction

Nowadays human life has closely been entangled with machineries and automotive applications that their emission and consumption is turned into a challenging issue worldwide. Any progress in the field of internal combustion chamber with responsive approach towards reduction of emission and fuel consumption is welcomed in R&D and research centers as long as its performance is elevated. Diesel engines are characterized with rich engine-out NOx emission that is proved having hazardous effects on human health [1,2]. On the other hand, these types of engine, although having the highest efficiency, waste considerable fuel's chemical energy and fail to capture the majority of the provided energy. One of the cost-effective methods is to use advanced injection system in the form of split injection, multiple injection, and pilot injection, thereby with this flexibility fuel is used at needed time [3-5].

It is believed that split injection can enhance the mixture quality thanks to electronically controlled common rail system that computer programs can manage the injection duty precisely and painstakingly [6,7]. It is reported that split injection is beneficial in reducing NOx content, fuel consumption, and engine noise [8]. Mobasheri [9] performed an investigation of narrow fuel spray and split injection on overall performance of a diesel engine. The main finding of the research showed that start of pilot (SOP) advancement makes more fuel accessible for mixing that explains more heat release rate. As a result of SOP advancing injection, locally fuel-lean mixture is prepared and the NOx and soot exceed the standard level. How et al. [10] in a relevant study conducted a study on injection timing and split injection on emission and combustion of diesel engine, therein the blend of biodiesel-diesel is considered. The application of B50 fuel in conjunction with multiple injection culminates in lowering NOx and smoke. Multiple injection was also addressed in recent researches such as the one by Park et al. [11] and also in Ref. [12]. It is pointed out that the start of combustion is affected by multiple injection while the combustion pressure of this type of injection is higher; meanwhile the latter study with focus on multiple injection revealed that it may lean out the mixture, which can considerably decrease soot concentration.

The exergy analysis is of concern since it is an index of the quality of energy or availability of energy that can be converted to useful work. In a combustion chamber of the engine, there are three sources of exergy destruction, the heat or energy wasted by the gases exiting from exhaust valve, wall heat flux, and spray fuel droplets that impinges the wall and miss being combusted. Another aspect of this study revolves around exergetic examination of the engine as different divergent split injection implemented. In recent years, couple of works have been performed with incorporation of the second law of thermodynamics in diesel engines [13-16], homogenous charge compression ignition (HCCI) engines [17], spark ignition (SI) engines [18, 19], and some of them are devoted to exergetic analyses of blended fuels in engines [20]. In the field of exergy evaluation, Kul and Kahraman [21] explored a diesel engine fueled with biodiesel-diesel-5% ethanol in terms of energy and exergy. As they concluded, D92B3E5 gave the highest exergy efficiency with 29.38%, and D100 has the better thermal and exergetic efficiency than that of blended fuels. Mahabadipour et al. [22] studied the exergy of exhaust flow in a diesel engine in an attempt to recover the waste energy. The exergetic analyze has taken place in crank-angle resolved base and it was indicated that the specific thermal exergy prevails at the primary period of the exhaust process.

The link between the mixture quality and exergy (or irreversibility) is a theme that little has been performed noticing the literature review. Consequently, unravelling the extricate mechanism of combustion-power generation interaction can be of paramount importance since this allows eradication of factors that lead to low efficiency of engines. This study tries to deal with an advanced split injection with two nozzles targeting with diverged included angles to combustion chamber. First, the uniformity of mixture, burned fuel mass fraction, rate of pressure rise is calculated, then the exergy terms are applied to energetic data. This way, an optimum case and the factors leading to gain the most useful work out of the given fixed amount of fuel can be recognized. The final goal is to prevent the heat or energy dissipation from the cylinder and convert the chemical potential of fuel to as much power as possible.

2. Thermodynamic evaluation

2.1. Injection description

The engine setup used for the numerical simulation [23] is equipped with VGT technology that allows high-pressure, precise, and flexible multiple injection at high engine speed. The injectors issue the fuel asynchronously with two pulses to the bowl and crevice consecutively. The amount of injected fuel mass is constant and considered fixed for the entire test for split and single injection in experimental work that is 37.43 mg/cycle at 2500 rpm. The lower nozzle angle is fixed at 140° with respect to –x axis and the upper nozzle for different cases make diffraction angle of the lower nozzle with 10°, 20°, 30° so making

150°, 160°, and 170° with –x direction. The fuel mass distribution and the time of injection is divided on 70%-30%, 80%-20%, and 90%-10% ratios and the span between two pulses (referred to as dwell time and signified by x in parenthesis) are in four levels of 5 CA, 10 CA, 15 CA, and 20 CA. The first pulse is injected through the lower-angled nozzle at 4 °CA BTDC carrying a share of fuel mass that is pursued by an interval before the second pulse begins with upper-angled nozzle. For better illustration, a schematic representation of diverged split injection is shown in Fig. 1. Different cylinder head position with regard to dwell time as well as the injection orientation of dual spray for typical 70 (x) 30 is displayed in Fig. 1b. Overall, the study is composed of 36 different cases to cover all injection modes. The portioning of fuel mass between pulses for diverse injection strategies in each cycle is mentioned in Table 1.

(a)

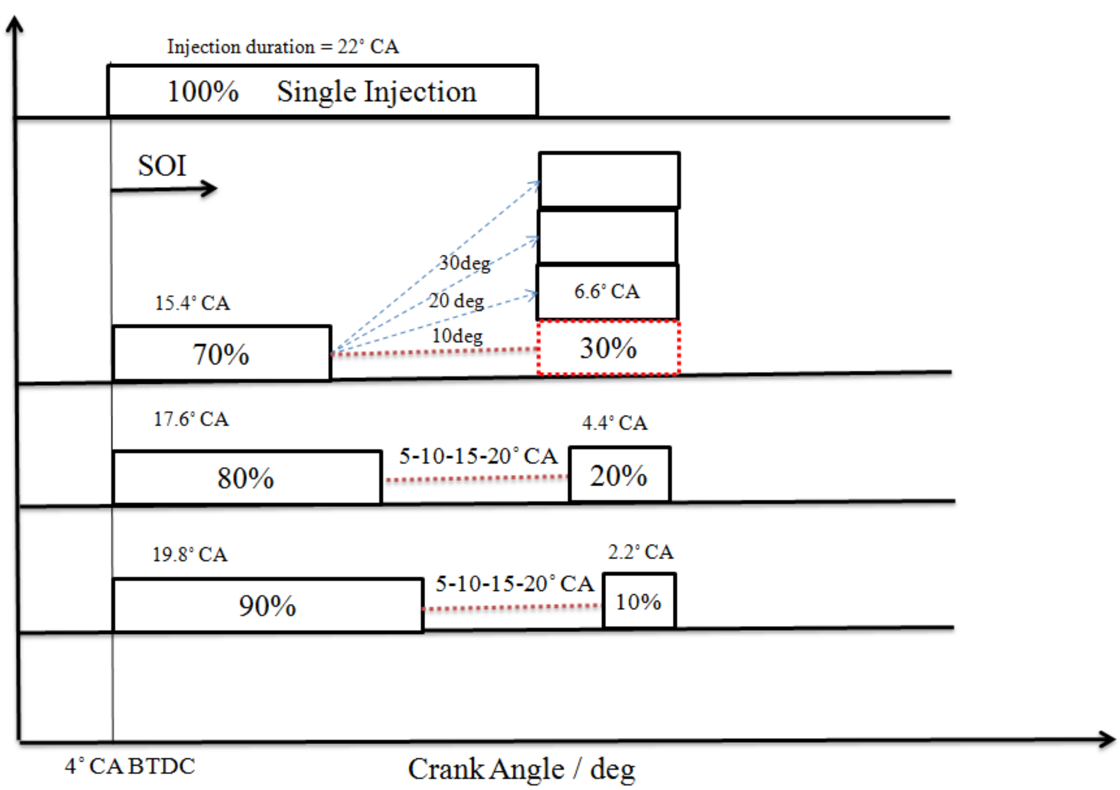

(b)

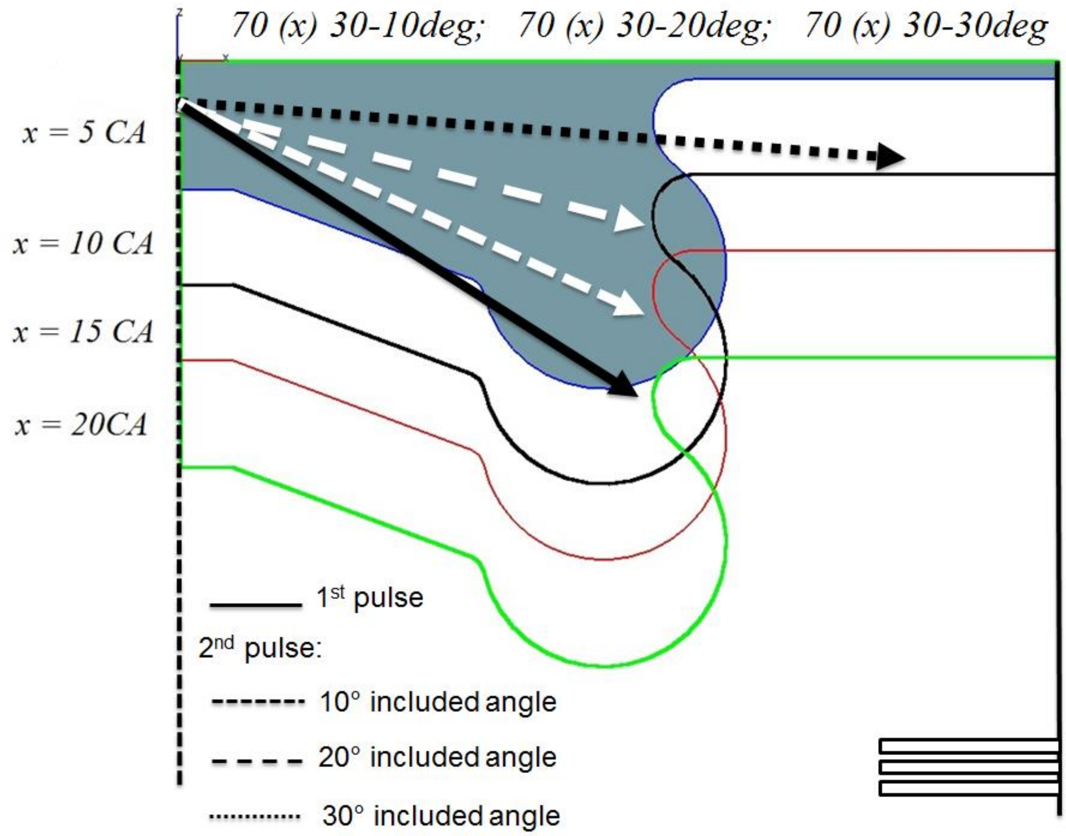

Fig. 1 (a) schematic representation of split injection, (b) typical 70 (x) 30 split injection

2.2. Energy modeling with CFD methodology

The finite volume (FV) method is used to solve the conservative set of Navier - Stokes equations in the discretized format of the flow domain. The SIMPLE (semi-implicit method for pressure-linked equations) algorithm is a reasonable choice to deal with the highly unsteady and turbulent flow of combustion phenomena [24]. For spray injection, the DDM (discrete droplet model) method [25] accounts for the evolution of spray in the chamber, therein similar droplets are taken together in parcels. The KH-RT breakup formulates the process of secondary atomization of droplets in spray simulation [26]. The k-ζ-f model is a successful turbulence closure particularly to meshes with the near wall non-dimensional distance (y^+) [27]. The step-size running procedure portraits the computational cost spent on calculations and the initial stage of calculation is conducted with $\Delta\alpha = 0.1$ CA subdivision. Accordingly for the compression and combustion phases the divisions are $\Delta\alpha = 1$ CA and $\Delta\alpha = 0.2$ CA. The under-relaxation factors are very important for the stability and convergence of numerical solution. These factors are set 0.6, 0.5, and 0.95 for momentum, pressure, and energy. The heat-up and evaporation required for the ignition and combustion is performed via the Dukowicz model with tuning constants of E1 = E2 = 1 [28]. The turbulent dispersion model and particle interaction model are activated for an accurate flow prediction within the combustion chamber. This is done by a stochastic dispersion model [29]. The detailed multi-zone ECFM-3Z combustion model is selected for the burning of the charge and chemical reaction responsible for production of species [30]. The initial and boundary conditions for an efficient modeling are tabulated in Table 2. The engine specifications are listed in Table 3.

In order to prove the reliability of the modeling in terms of accuracy of the achieved results, Fig. 2 is provided wherein mean pressure and accumulative heat release (AHR) of the computed and measured data [23] are compared for the single injection of the engine at 2500 rpm engine speed. The max. error is seen at peak pressure (~368 °CA) which is still less than 3% and it can be attributable to evaporation rate and breakup simulation models during initial combustion phase as well as experimental setup uncertainties. Other than that, the model is able to predict the engine behavior acceptably.

(a)

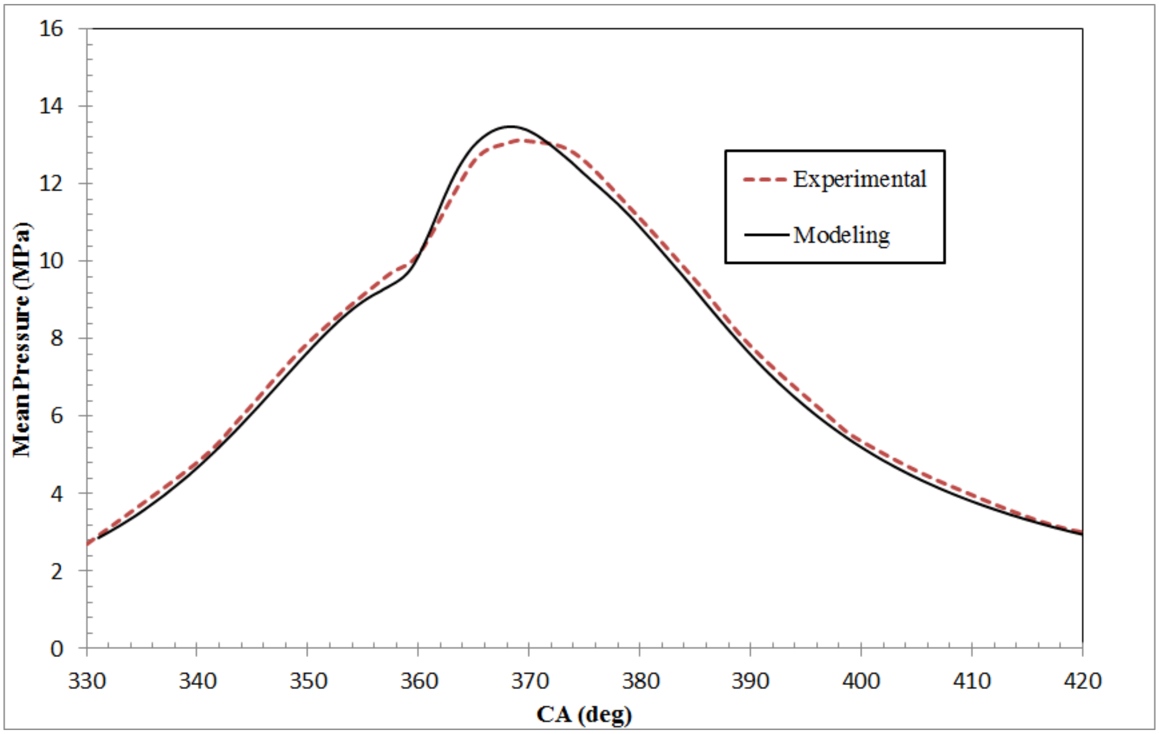

(b)

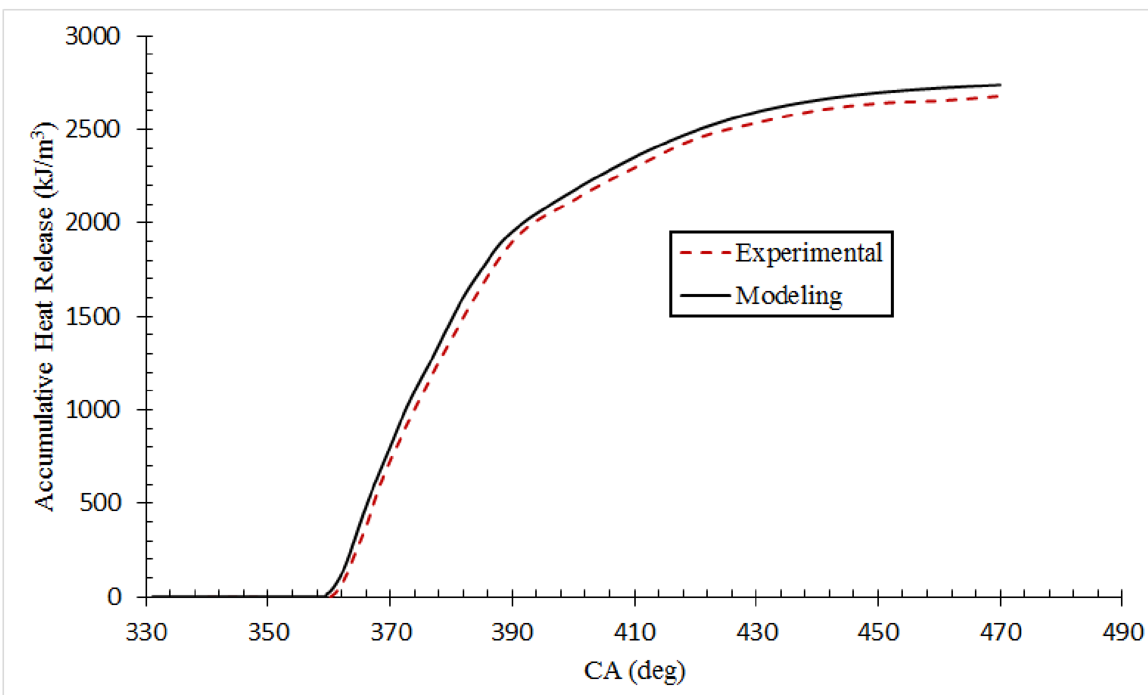

Fig. 2 Comparison of computed data with experimental results for (a) pressure, (b) AHR

2.3. Computation of exergy

Cylinder exergy balance can be formulated as follow [31]:

$$\frac{dA_{cyl}}{d\phi} = \frac{\dot{m}_{in} b_{in}^{tm} - \dot{m}_{out} b_{out}^{tm}}{N} - \frac{dA_l}{d\phi} - \frac{dA_w}{d\phi} + \frac{dA_f}{d\phi} - \frac{dI}{d\phi} \quad (1)$$

where $\dot{m}_{in}$ is the incoming flow rate from the inlet manifold and consists of air and $\dot{m}_{out}$ is the outlet mass flow to the outlet manifold, b_{in}^{tm} and b_{out}^{tm} refer to the flow thermo-mechanical exergy of incoming and outgoing cylinder mass flow rates [31]:

$$b^{tm} = (h - h_0) - T_0(s - s_0) \quad (2)$$

$\frac{dA_l}{d\phi}$ is the heat transfer exergy to the cylinder walls on the basis of crank angle degree. It can be given as follow [31]:

$$\frac{dA_l}{d\phi} = \frac{dQ_l}{d\phi}\left(1 - \frac{T_0}{T_{cyl}}\right) \quad (3)$$

$\frac{dQ_l}{d\phi}$ is the heat transfer rate to the cylinder walls on the basis of crank angle degree and T_{cyl} is the instantaneous temperature of the cylinder gasses, which are available from the first law analysis. $\frac{dA_w}{d\phi}$ represents the indicated work transfer. In fact, it can be defined as the value of output exergy from the cylinder associated with the indicated work [31]:

$$\frac{dA_w}{d\phi} = (P_{cyl} - P_0)\frac{dV}{d\phi} \quad (4)$$

where $\frac{dV}{d\phi}$ states the rate of cylinder volume change based on crank angle degree and P_{cyl} is the instantaneous cylinder pressure which both are calculable by the first law analysis in the engine processes. The burned fuel exergy on the crank angle basis can be calculated as follow [31]:

$$\frac{dA_f}{d\phi} = \frac{dm_{fb}}{d\phi} a_{fch} \tag{5}$$

a_{fch} represents the chemical fuel exergy. The chemical exergy of substances in the environment (e.g. fuel, sulfur, combustion products such as NO or OH, etc.) can be evaluated by considering an idealized reaction of the substance with others with the known chemical exergies [32]. This chemical exergy of the fuel can be expressed on a molar basis as follow [31, 32]:

$$\bar{a}_{fch} = \bar{g}_f(T_0, P_0) - \left(\sum_p x_p \bar{\mu}_p^0 - \sum_r x_r \bar{\mu}_r^0 \right) \tag{7}$$

where index *p* denotes products (CO_2, H_2O, CO, etc.) and index *r* is the reactants (fuel and O_2) of the (stoichiometric) combustion process, T_0 and P_0 are the dead state temperature and pressure, and the over bar denotes properties on mole basis. For liquid hydrocarbon fuels with molecular formulation of C_zH_y, the chemical exergy of fuel can be expressed as follows (on a kg basis) [33]:

$$a_{fch} = LHV \left(1.04224 + 0.011925 \frac{y}{z} - \frac{0.042}{z} \right) \tag{8}$$

where *LHV* is the fuel lower heating value.

The $dI/d\phi$ term in equation (1) represents the rate of irreversibility production in the cylinder, which includes combustion, viscous loss, turbulence, mixing and etc. According to Dunbar and Lior [34], a combustion reaction has four major sources of internal irreversibility. They are:

- A chemical diffusion process in which air and fuel molecules are drawn together.
- Combustion of the fuel-air mixture (thermo-chemical reaction).
- Internal energy exchange through molecular collisions amongst the products and radiation heat transfer amongst product constituents due to unequal heat distribution.
- Mixing process whereby reactants mix before combustion, and products mix with reactants during combustion due to proximity.

Since the contribution of combustion in irreversibility production is more than 90% [35, 36], in the present study, only the combustion irreversibility is taken into evaluate the in-cylinder irreversibilities. The combustion irreversibilities on the crank angle basis can be given as [37]:

$$\frac{dI}{d\phi} = -\frac{T_0}{T_{cyl}} \sum_j \mu_j \frac{dm_j}{d\phi} \tag{9}$$

where subscript *j* includes all reactants and products. For ideal gases, $\mu_j = g_j$ and for the fuel $\mu_f = a_{fch}$.

Aforementioned equations can be solved by the numerical methods in order to evaluate the second-law terms in an engine cycle.

3. Results and discussion

3.1. Energetic evaluation

The mixing process of fuel droplets and air is a crucial mechanism in having an efficient combustion, so the uniformity and homogeneity of mixture is quantified and scaled by "air-fuel uniformity index" as follows:

$$UI = 1 - \frac{1}{n}\sum_{i=1}^{n}\frac{\sqrt{(w_i - w)^2}}{w} \qquad (10)$$

where w_i is the equivalence ratio in the *i*-th cell of the meshed domain in the combustion chamber. The scaled quantity of UI varies between 0-1 denoting consummate uniformity when UI = 1. The different injection schemes for 36 different injection cases where one of the portions of injection between the first and second pulses, injection angles, or dwell times is meant to let achieving the optimum fuel distribution and hence use the most of fuel energy's potential.

Fig. 3 diagram shows the peak UI variation for different injection strategies of this study. In the first place, it can be observed that the highest UI belongs to 70 (5) 30-30deg and the homogeneity of mixture tends to reduce with dwell time from 5→20 as the polynomial interpolation curve indicates. This is due to well-distributed portions of fuel between the first and second pulses while the divergent injection angle is such timed to target the bowl area after 5 CA dwell time, so that the wall-impingement would be minimized. On the other hand, a reverse trend is spotted with 70 (5) 30-10deg and the more dwell time is spent, the more mixture uniformity is resulted (as the poly. curve interpolation suggests). What is more, it can be stated that in general 70 (x) 30 > 80 (x) 20 > 90 (x) 10 is true in terms of UI wherein this uniformity aides towards better fuel capacity utilization in the form of stoichiometric combustion of the system.

Fig. 3 Peak UI vs. dwell time for different split injection schemes

Subsequently, the flow behavior of the cylinder influences the subsequent combustion phenomena and the peak in-cylinder temperature is plotted for different injection modes in Fig. 4. There is a clear correspondence between uniformity and temperature for different split injection modes. The temperature plot almost follows the UI pattern with the highest temperature happening at 70 (5) 30-30deg (2011.58 K) whereas the lowest one can be noted for the 90 (5) 10-10deg with 1721.65 K. The reason for low mixture uniformity and temperature of 90 (5) 10-10deg is that the distribution of fuel portion is limited and approaches to a single injection. The uniformity of mixture with dwell time is increasing for 70 (x) 30-10deg, this leads to a more complete combustion and oxidation of hydrocarbon fuel, therefore as seen in Fig. 4 the cylinder temperature increases with dwell time. In this case, dwell time acts as an opportunity for droplets to diffuse in air in different chamber areas. Among increasing pattern of 70 (x) 30-10deg and declining pattern of 70 (x) 30-30deg, the maximum temperature for 70 (x) 30-20deg occurs at x= 15 CA.

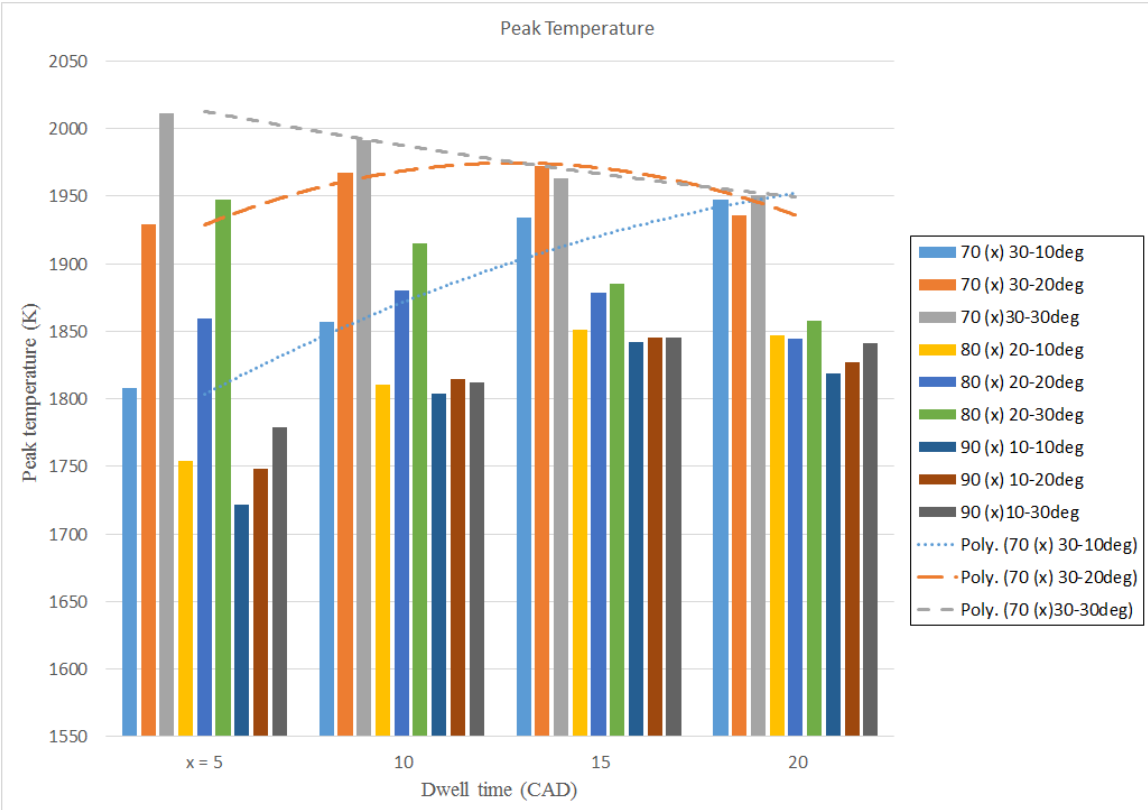

Fig. 4 Peak in-cylinder temperature vs. dwell time for different split injection schemes

The maximum burned fuel mass fraction at 840 CA ATDC is demonstrated in Fig. 5 for different split injection modes. Again, for the case of 70 (x) 30, the cylinder contains more burned fuel than other fuel portioning policies. However, other than 80(x) 20-30deg, other cases project a growing concentration of burned fuel with dwell time increment. This is related to a more time given for fuel droplets burning in the greater time span of dwell time between injection pulses, this issue is evident in the bar chart of x = 20 CA when all burned fuel fractions of different cases have got closer to each other.

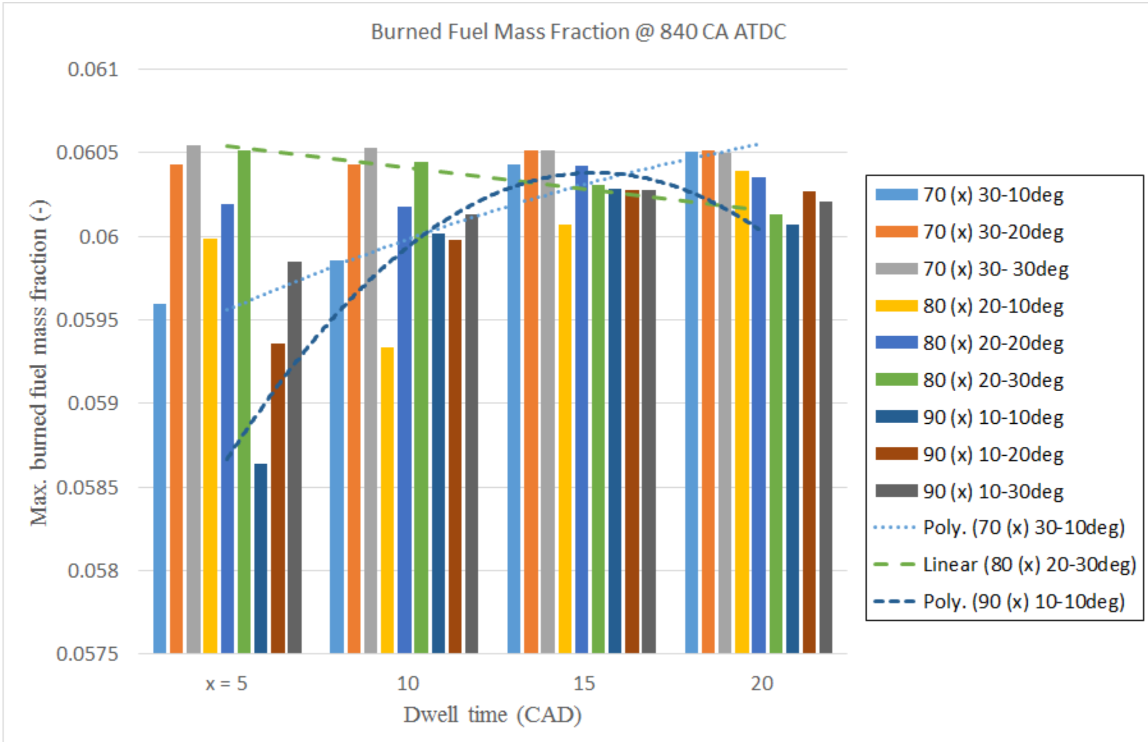

Fig. 5 Peak burned fuel mass fraction vs. dwell time for different split injection schemes

The more burned fuel mass fraction indicates that the system is better empowered to utilize the chemical potential of the hydrocarbon fuel.

The cylinder pressure is another parameter of significance in measuring the energetic performance of the engine that comes with the explosive nature of compression-ignition of diesel. In this regard, the pressure and rate of pressure rise (RPR) for different injection plans are displayed in Fig. 6 with respect to CA. The RPR is calculated in 4 intervals step with central differencing derivatives:

$$RPR = \frac{dP_i}{d\theta} = \frac{P_{i+2} - P_{i-2}}{4h} \qquad (11)$$

P denotes the discrete calculated pressure, h is the change in CA step size between two consecutive runs, so in our case, $h = \Delta\alpha$.

According to Fig. 6, the peak RPR (907.67 kPa/deg) and pressure (13.97 MPa) occurs for 80-20 fuel mass distribution and the lowest is for 70-30. This shows that a good mixing procedure of fuel and oxidizer for 70-30 injection is a factor for a gradual and qualified combustion that can enhance the burning rate and chemical kinetics; therein the knock can be avoided. The higher chamber pressure of 70-30 injection mode during post combustion phase (i.e. mixing controlled combustion phase) implies the better engine torque and its overall performance in terms of the first law of thermodynamics.

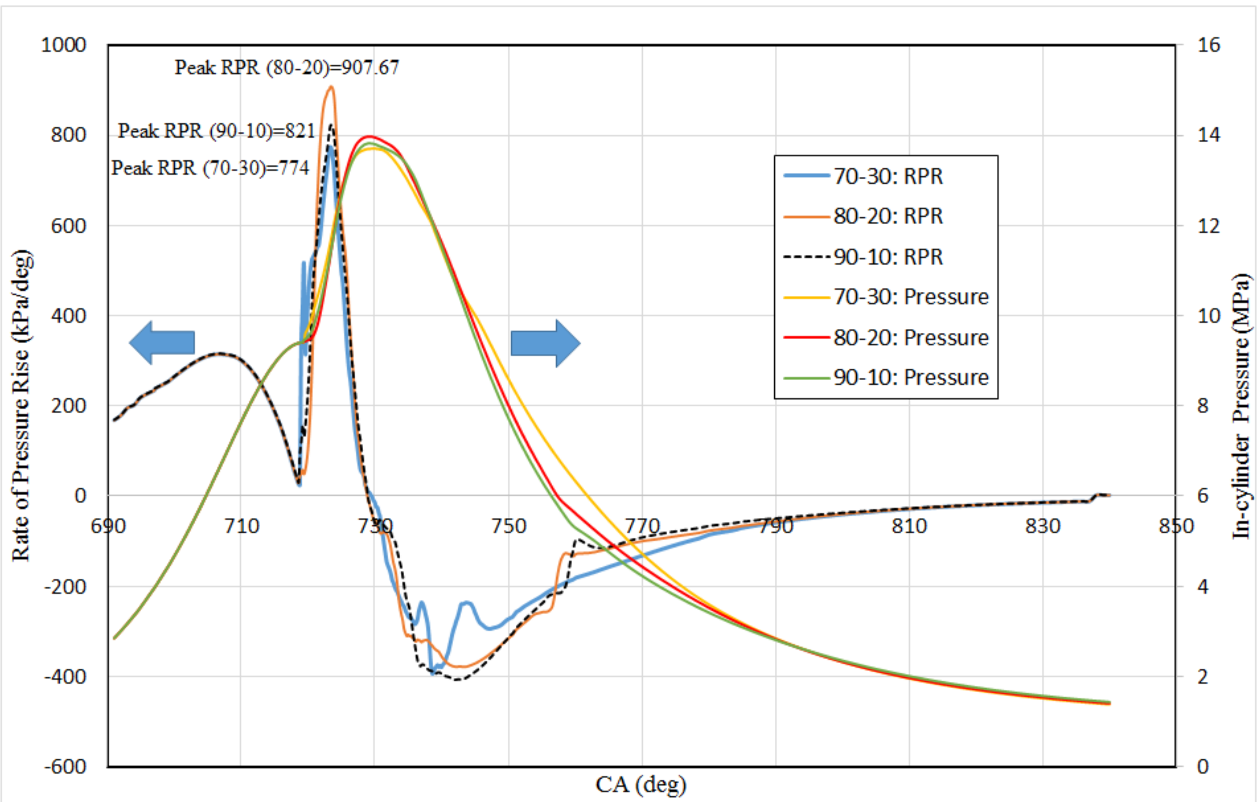

Fig. 6 Pressure and RPR variation with CA for 70-30, 80-20, and 90-10 injection plans

3.1. Exergetic evaluation

The second law of thermodynamics provides a platform for estimation of the energy quality in a given system. In current research, we are interested to analyze the influence of advanced split injection on exergy terms, thereby find the best case for extracting the most useful work out of the combustion chamber. The indicated work exergy in the accumulative (time-integrated) form with respect to CA for different advanced injection modes is presented in Fig. 7a. As seen, the work exergy is increasing with CA to deliver the mechanical rotation power at the end period of thermodynamic cycle.

With reference to Table 4, the highest and the lowest amount of IMEP as expected goes to 70 (5) 30-30deg and 90 (5) 10-10deg with 5.77 bar and 5.334 bar, respectively. This dominant IMEP that stems from better uniformity of mixture and thus better combustion for 70 (5) 30-30deg. Moreover, for the accumulative work exergy (AWE), the following order of $AWE_{(70\text{-}30)} > AWE_{(80\text{-}20)} >> AWE_{(90\text{-}10)}$ is seen that is acceptable since the distribution of fuel proportion between pulses allows for better utilization of fuel energy. Based on Fig. 7b, which shows variation of peak accumulated work exergy with dwell time, the maximum work exergy is associated with 70 (x) 30-30deg. For that, increasing the dwell time gives the reduction in work exergy that is in close agreement with the trend observed for UI in Fig. 3. That is to say, increasing the dwell time gives away the chance to turn the provided chemical energy to work mainly because the fuel jet to wall impingement with dwell time increment. For the injection cases of 80-20 and 90-10, the dwell time plays a positive role in gaining an efficient fuel droplet diffuse in oxidizer, so the peak accumulated work rises with dwell time.

(a)

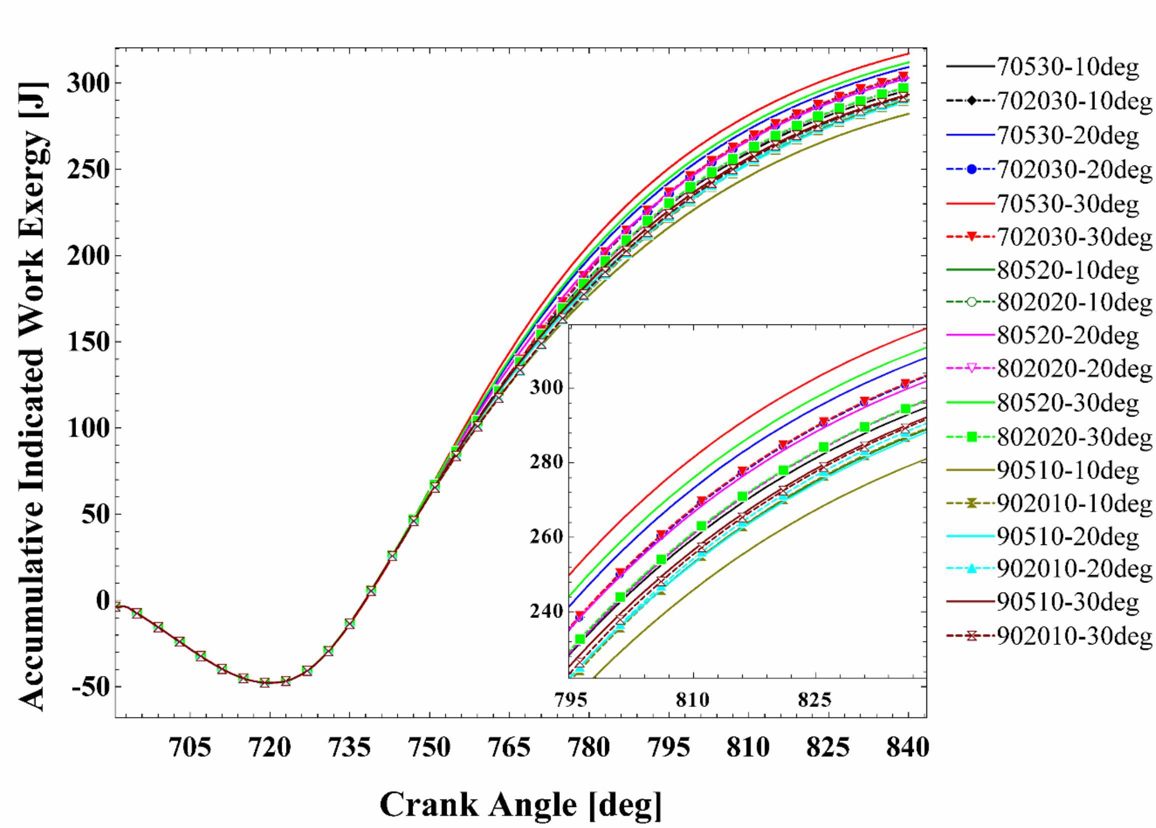
Accumulative Indicated Work Exergy [J]
Crank Angle [deg]
70530-10deg
702030-10deg
70530-20deg
702030-20deg
70530-30deg
702030-30deg
80520-10deg
802020-10deg
80520-20deg
802020-20deg
80520-30deg
802020-30deg
90510-10deg
902010-10deg
90510-20deg
902010-20deg
90510-30deg
902010-30deg

(b)

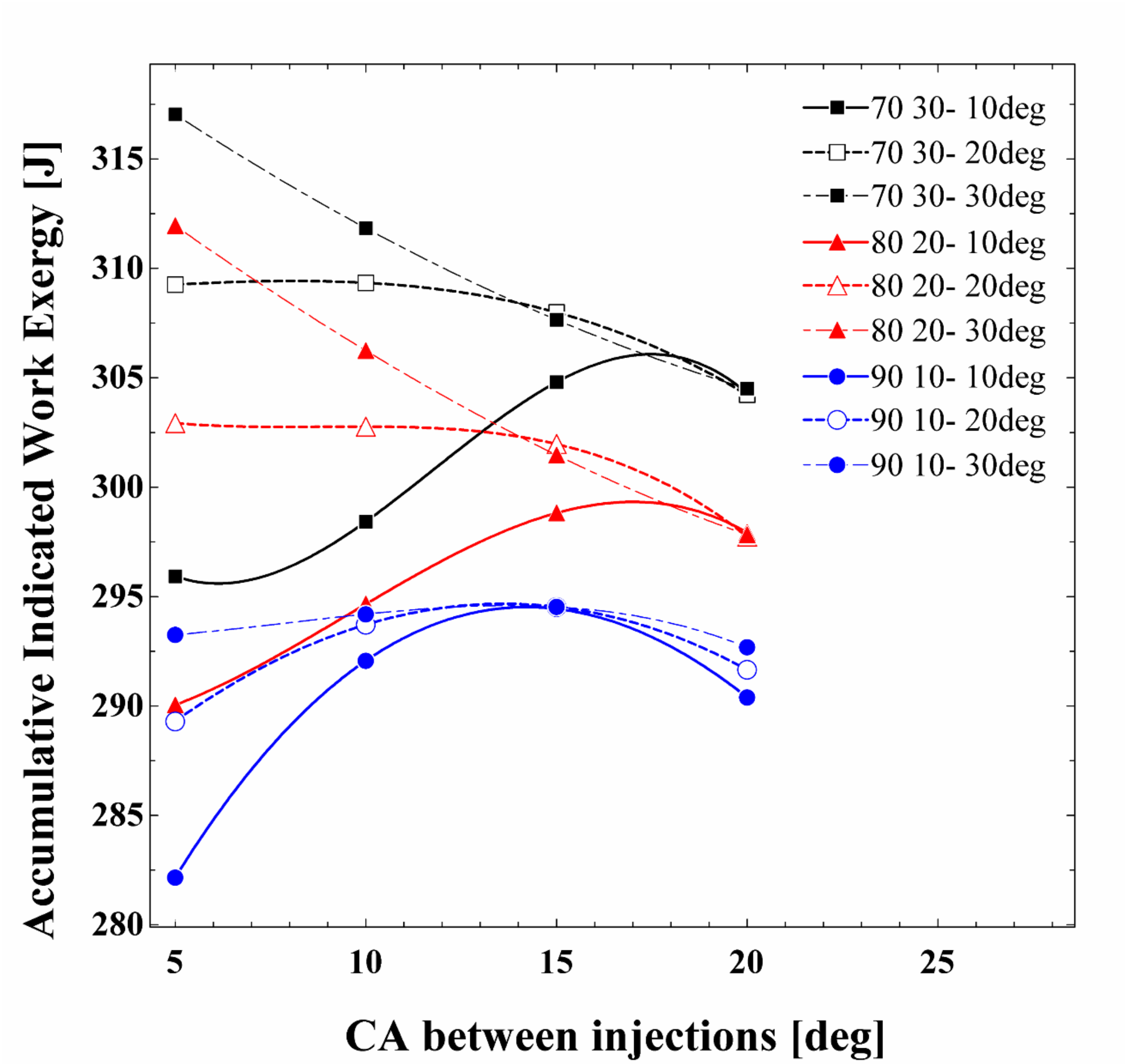

Fig. 7(a) variation of accumulative work exergy with CA, (b) peak accumulative work exergies with dwell time for different injection modes

The variation of accumulated heat loss exergy (AHLE) with CA for different split injection modes is illustrated in Fig. 8a. From Fig. 8a, the most convertible heat comes from 70 (5) 30-30deg and the lowest AHLE corresponds to 90 (5) 10-10deg. The reason lies in the fact that majority of fuel is burnt at once with little opportunity to change the provided heat. In Fig. 8b, the peak AHLE against dwell time is depicted for various injection plans. It is clear that the higher heat loss exergy goes for 70-30, then 80-20, and finally the lowest accumulative heat exergy is for 90-10. As mentioned before, 70-30 strategy allocates suitable amount of fuel between pulses and this action makes an efficient combustion with higher temperature than in the single injection, which increases thermal waste. For 30deg divergent split injection, for all 70-30, 80-20, and 90-10 injections, the AHLE are decreasing with dwell time, although the rate of decrement for 70-30 is more noticeable. It is mainly originated from more spray cylinder wall interaction and more importantly, the shift of second pulse injected fuel's combustion towards EVO timing.

(a)

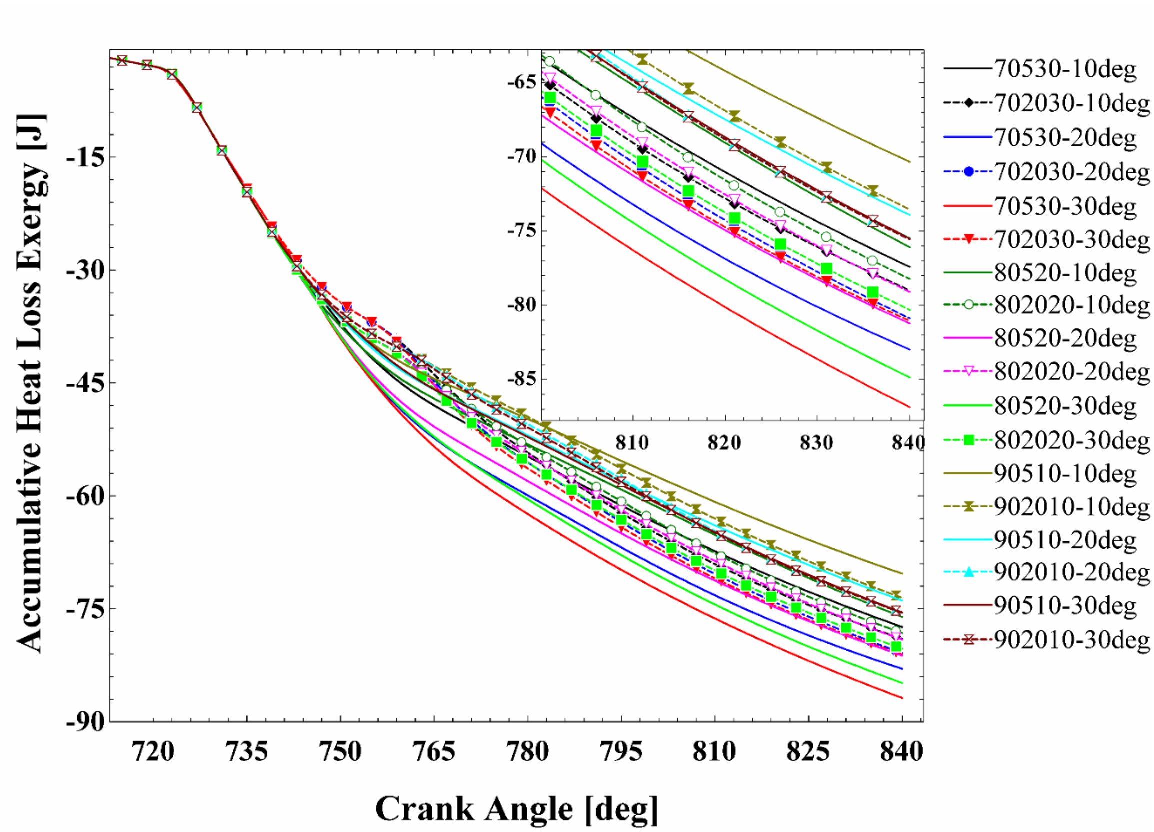

(b)

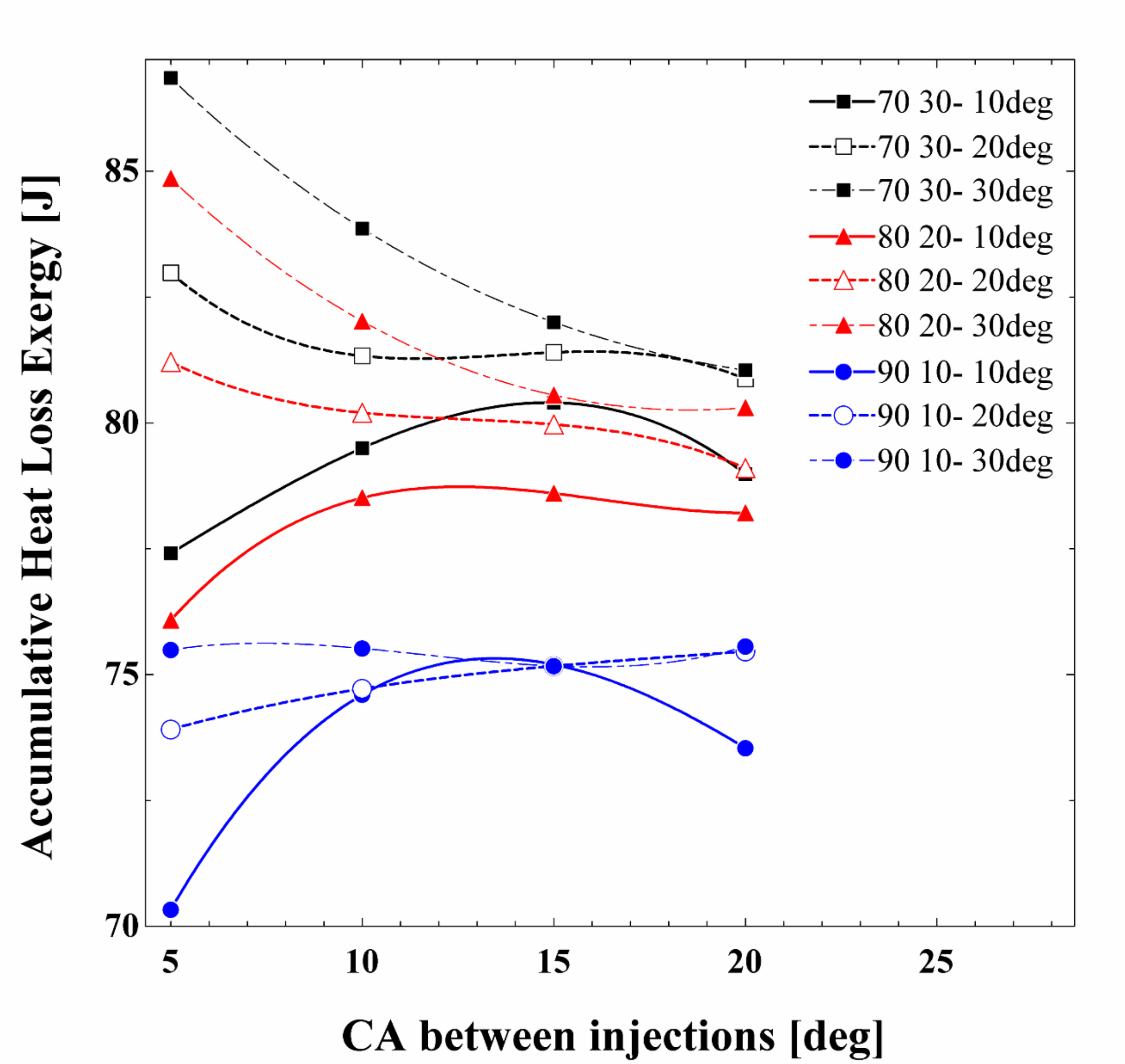

Fig. 8(a) variation of accumulative heat loss exergy with CA, (b) peak accumulative heat loss exergies with dwell time for different injection modes

Thermo-mechanical exergy with CA and exhaust thermo-mechanical exergy with dwell time is represented in Fig. 9 for different operational split injection modes. The cases that have a shorter time between two pulses show one peak thermo-mechanical exergy while longer dwell time exhibit two peak curves and usually their thermo-mechanical exergies are lower. It is clearly demonstrated that the thermo-mechanical exergy of 70 (5) 30-30deg dominates with 439 J. Three chief reasons can explain this: (a) the fuel mass proportion is properly divided between two pulses, (b) 30deg injection angle between two nozzles provide a proper spatial distribution of fuel spray, (c) the short dwell time (~5 °CA) prevents coincidence of the second injection combustion with EVO timing.

The missed chance for applying the exhausted gas from chamber to thermo-mechanical exergy for 90-10 is greater and much of the thermal energy is lost from the exhaust valve. The exhaust thermo-mechanical exergy expresses the exergy content that leaves the cylinder from the exhaust valve, which could be used to exert power on piston or converted to work, however this chance is missed. The general observed trend from Fig. 9b is the increase of exhaust thermo-mechanical exergy with dwell time due to shift of combustion towards the expansion (power) stroke. Referring to Fig. 5, one notes the higher burned mass fraction of 70 (5) 30-30deg that is an indication of more reactivity of fuel components with oxidizer. This shows that much more of fuel has burned, thereby more reaction species are released as a result of combustion which gives way to more thermo-mechanical exergy (the opposite trend goes for 90 (5)10-10deg). According to Fig. 9b, the necessity for adopting the proper injection mode can be confirmed since a 9.5% reduction in exhaust thermo-mechanical exergy occurs when 70 (5) 30-30deg is used instead of 90 (20) 10-10deg, thereby a considerable save of fuel chemical potential is created in convertibility to useful work output.

(a)

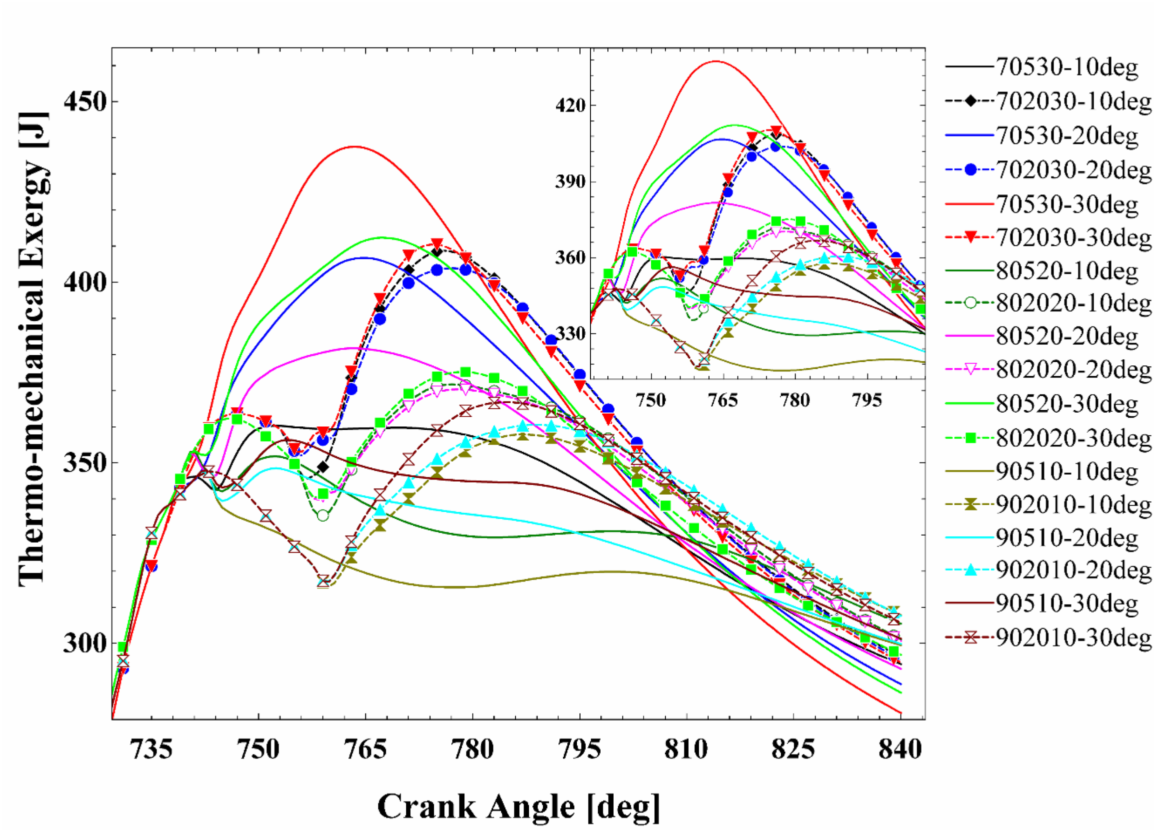

Thermo-mechanical Exergy [J]
450
400
350
300
735
750
765
780
795
810
825
840
Crank Angle [deg]
420
390
360
330
750
765
780
795
70530-10deg
702030-10deg
70530-20deg
702030-20deg
70530-30deg
702030-30deg
80520-10deg
802020-10deg
80520-20deg
802020-20deg
80520-30deg
802020-30deg
90510-10deg
902010-10deg
90510-20deg
902010-20deg
90510-30deg
902010-30deg

(b)

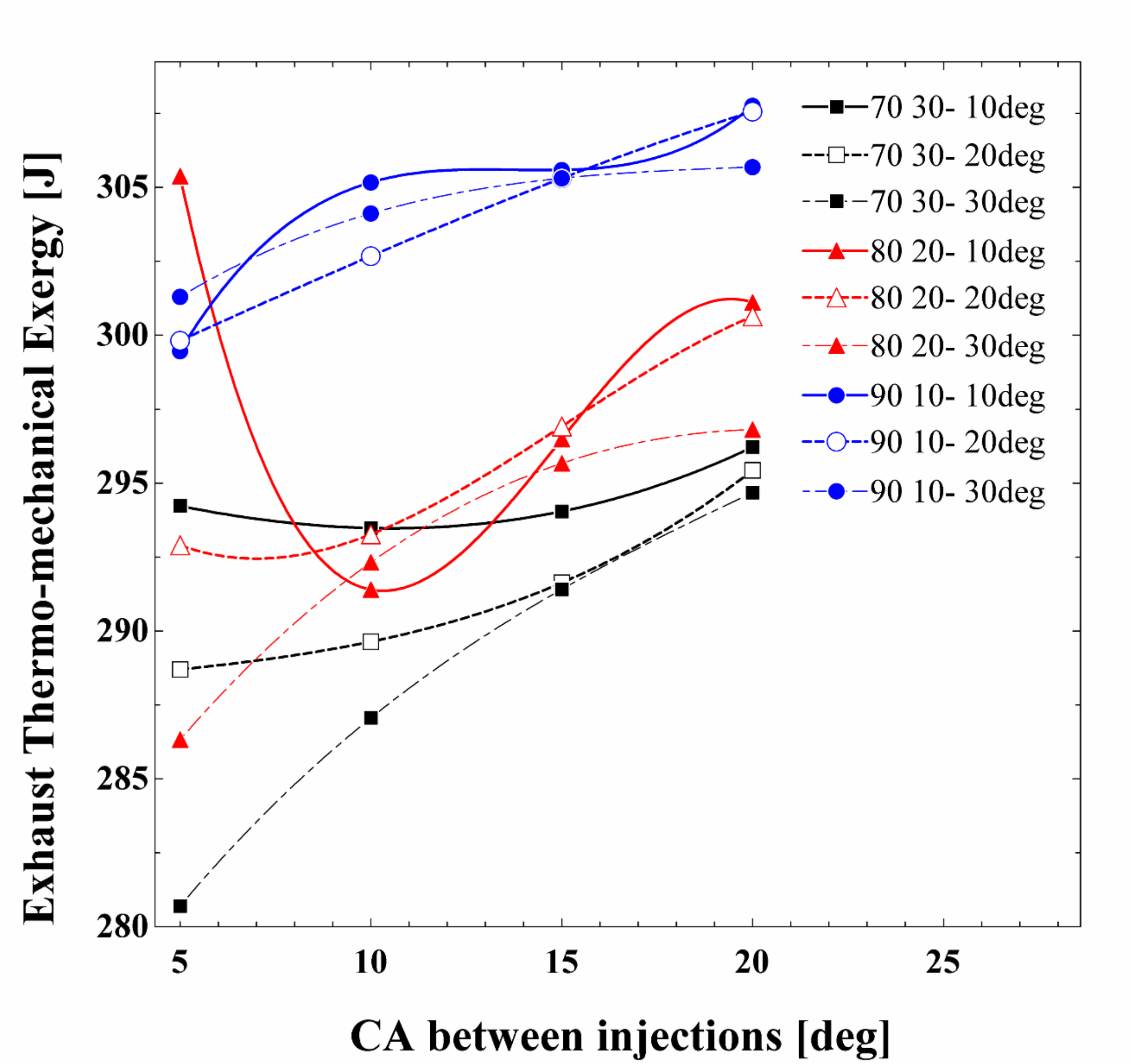

Fig. 9(a) variation of thermo-mechanical exergy with CA, (b) exhaust thermo-mechanical exergy with dwell time for different injection modes

The irreversibility rate variation with CA evolution is shown in Fig. 10a for different injection modes. Taken Fig. 5 into consideration, the high irreversibility rate for 80 (20) 20-30deg can be explained since greater PRP leads to the rapid burning rate and intense combustion which accordingly increases the irreversibility of the process. The accumulative irreversibility with respect to dwell time for different injection modes is presented in Fig. 10b. It is found that, in contrast to exergy terms, accumulated irreversibility of 90-10 is prevalent, next comes 80-20, and 70-30 strategies. The maximum accumulative irreversibility occurs at 90 (10) 10-20deg and the lowest amount at 70 (5) 30-30deg, a case that gave the most UI. The similar result more recently reported in [38], where the stoichiometric combustion culminated in the lowest level of exergy destruction fraction. In addition, as it is recorded in Fig. 4, the 70-30 fuel injection scheme generates the greatest in-cylinder temperature and according to Ref. [39], the higher cylinder temperature would decrease the irreversibility. Therefore, based on Fig. 10b, the lowest irreversibility is observed for 70-30 and the most irreversibility can be associated to 90-10 due to lower cylinder temperature. The reason is such explained that if the cylinder temperature increases, the heat transfer from hot gases to yet unburned mixture would decrease. In conclusion, it can be summarized that mixture uniformity is a primary parameter to reduce the irreversibility of a combustion system, therefore avoid the waste energy in the form of lost heat.

(a)

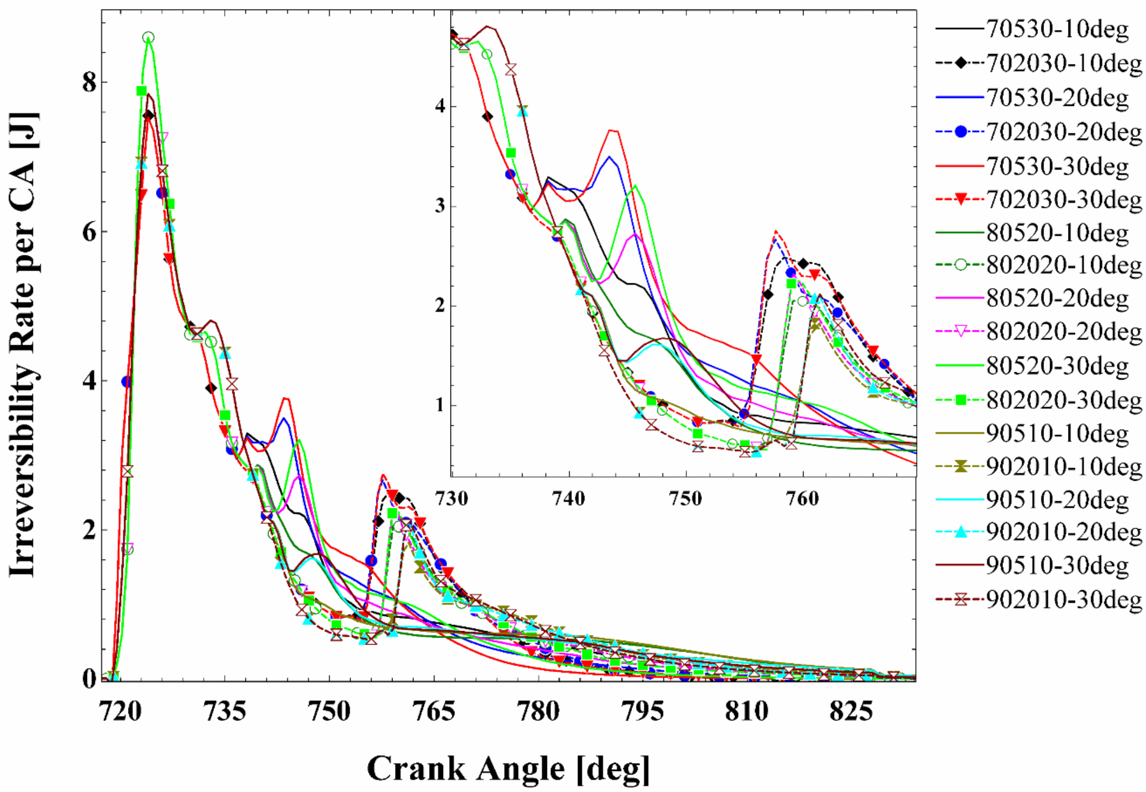
Irreversibility Rate per CA [J]
Crank Angle [deg]
0
2
4
6
8
720
735
750
765
780
795
810
825
730
740
750
760
1
2
3
4
70530-10deg
702030-10deg
70530-20deg
702030-20deg
70530-30deg
702030-30deg
80520-10deg
802020-10deg
80520-20deg
802020-20deg
80520-30deg
802020-30deg
90510-10deg
902010-10deg
90510-20deg
902010-20deg
90510-30deg
902010-30deg

(b)

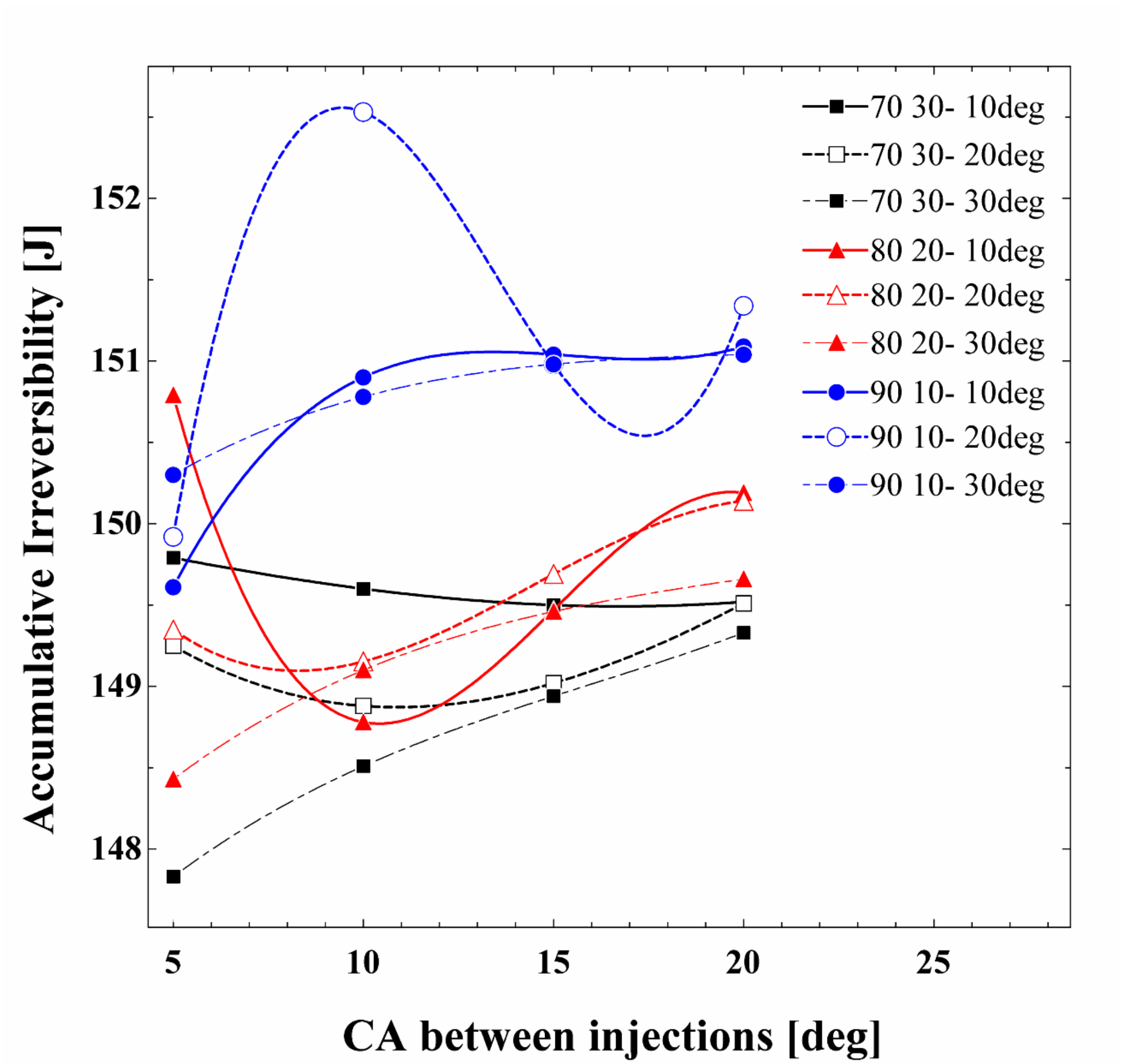

Fig. 10(a) variation of irreversibility rate with CA and (b) accumulative irreversibility with dwell time for different injection modes

4. Conclusion

In this work, an advanced split injection is undertaken wherein the responsibility of the injection for the first and second pulses is with two discrete nozzles whose angles aim to different zones of combustion chamber and this helps covering wider segments of cylinder. In the modern injection two mechanisms of various dwell time and nozzle included angles are predicted to homogenize the air-fuel mixture. The objective of the research was to determine if there is any correlation between the uniformity of mixture (obtained by split injection) and exergy concept. The results from the CFD code of AVL-FIRE is incorporated with the in-house developed FORTRAN code for exergy analysis, whereupon it is revealed that the case (70 (5) 30 -30deg) could give the highest uniformity and burned fuel mass fraction leading to maximum accumulative work/heat exergy and thermo-mechanical exergy. On the opposite side, the 90 (5) 10-10deg strategy shows the weakest performance due to its closeness to a single injection scheme.

According to findings of this research, the single injection (mostly done in conventional diesel engines) has a very big exhaust thermo-mechanical exergy, which means a great deal of the potential energy is wasted without being tapped or utilized as to propel a device. Other than that, it is proved that the irreversibility rate is correlated with RPR such that RPR of 80-20 mode has the highest peak of 907.67 kPa/deg leading to the highest irreversibility rate of 8.6 J/deg, while accumulated irreversibility is reversely proportionate with in-cylinder temperature. It is also concluded that taken a recommended split injection ratio (70 (5) 30-30deg) cause prevention of waste in thermo-mechanical exergy by 9.5%.

References

[1] Li, N., Hao, M., Phalen, R.F., Hinds, W.C. and Nel, A.E., 2003. Particulate air pollutants and asthma: a paradigm for the role of oxidative stress in PM-induced adverse health effects. *Clinical Immunology*, *109*(3), pp.250-265.

[2] Zhang, J.J., McCreanor, J.E., Cullinan, P., Chung, K.F., Ohman-Strickland, P., Han, I.K., Järup, L. and Nieuwenhuijsen, M.J., 2009. Health effects of real-world exposure to diesel exhaust in persons with asthma. *Research report (Health Effects Institute)*, (138), pp.5-109.

[3] Yang, K., Yamakawa, H., Nishida, K. and Ogata, Y., 2018. CHARACTERISTICS OF FREE SPRAY DEVELOPMENT, MIXTURE FORMATION, AND COMBUSTION UNDER HIGH-PRESSURE SPLIT INJECTION. *Atomization and Sprays*, *28*(3).

[4] Mendez, S. and Thirouard, B., 2009. Using multiple injection strategies in diesel combustion: potential to improve emissions, noise and fuel economy trade-off in low CR engines. *SAE International Journal of Fuels and Lubricants*, *1*(1), pp.662-674.

[5] Liu, H.F., Mao, B., Liu, J.L., Zheng, Z.Q. and Yao, M.F., 2018. Pilot injection strategy management of gasoline compression ignition (GCI) combustion in a multi-cylinder diesel engine. *Fuel*, *221*, pp.116-127.

[6] Mobasheri, R. and Peng, Z., 2013. CFD investigation into diesel fuel injection schemes with aid of Homogeneity Factor. *Computers & Fluids*, *77*, pp.12-23.

[7] Husberg, T., Denbratt, I. and Karlsson, A., 2008. *Analysis of advanced multiple injection strategies in a heavy-duty diesel engine using optical measurements and CFD-simulations* (No. 2008-01-1328). SAE Technical Paper.

[8] Busch, S., Zha, K. and Miles, P.C., 2015. Investigations of closely coupled pilot and main injections as a means to reduce combustion noise in a small-bore direct injection Diesel engine. *International Journal of Engine Research*, *16*(1), pp.13-22.

[9] Mobasheri, R., 2017. Influence of narrow fuel spray angle and split injection strategies on combustion efficiency and engine performance in a common rail direct injection diesel engine. *International Journal of Spray and Combustion Dynamics*, *9*(1), pp.71-81.

[10] How, H.G., Masjuki, H.H., Kalam, M.A. and Teoh, Y.H., 2018. Influence of injection timing and split injection strategies on performance, emissions, and combustion characteristics of diesel engine fueled with biodiesel blended fuels. *Fuel*, *213*, pp.106-114.

[11] Park, S.H., Kim, H.J. and Lee, C.S., 2016. Effect of multiple injection strategies on combustion and emission characteristics in a diesel engine. *Energy & Fuels*, *30*(2), pp.810-818.

[12] Mobasheri, R., Peng, Z. and Mirsalim, S.M., 2012. Analysis the effect of advanced injection strategies on engine performance and pollutant emissions in a heavy duty DI-diesel engine by CFD modeling. *International Journal of Heat and Fluid Flow*, *33*(1), pp.59-69.

[13] Taghavifar, H., Khalilarya, S. and Jafarmadar, S., 2015. Exergy analysis of combustion in VGT-modified diesel engine with detailed chemical kinetics mechanism. *Energy*, *93*, pp.740-748.

[14] Taghavifar, H., Khalilarya, S., Mirhasani, S. and Jafarmadar, S., 2014. Numerical energetic and exergetic analysis of CI diesel engine performance for different fuels of hydrogen, dimethyl ether, and diesel under various engine speeds. *International Journal of Hydrogen Energy*, *39*(17), pp.9515-9526.

[15] Nemati, A., Barzegar, R. and Khalilarya, S., 2015. The effects of injected fuel temperature on exergy balance under the various operating loads in a DI diesel engine. *International Journal of Exergy*, *17*(1), pp.35-53.

[16] Taghavifar, H., Khalilarya, S. and Jafarmadar, S., 2015. Three-dimensional energetic and exergetic analysis of the injection orientation of DI diesel engine under different engine speeds. *Energy Science & Engineering*, *3*(4), pp.360-370.

[17] Jafarmadar, S. and Nemati, P., 2016. Exergy analysis of diesel/biodiesel combustion in a homogenous charge compression ignition (HCCI) engine using three-dimensional model. *Renewable energy*, *99*, pp.514-523.

[18] Nemati, A., Fathi, V., Barzegar, R. and Khalilarya, S., 2013. Numerical investigation of the effect of injection timing under various equivalence ratios on energy and exergy terms in a direct injection SI hydrogen fueled engine. *international journal of hydrogen energy*, *38*(2), pp.1189-1199.

[19] Fathi, V., Nemati, A., Khalilarya, S. and Jafarmadar, S., 2011. The effect of the initial charge temperature under various injection timings on the second law terms in a direct injection SI hydrogen engine. *international journal of hydrogen energy*, *36*(15), pp.9252-9259.

[20] Krishnamoorthi, M. and Malayalamurthi, R., 2018. Availability analysis, performance, combustion and emission behavior of bael oil-diesel-diethyl ether blends in a variable compression ratio diesel engine. *Renewable Energy*, *119*, pp.235-252.

[21] Sayin Kul, B. and Kahraman, A., 2016. Energy and exergy analyses of a diesel engine fuelled with biodiesel-diesel blends containing 5% bioethanol. *Entropy*, *18*(11), p.387.

[22] Mahabadipour, H., Srinivasan, K.K., Krishnan, S.R. and Subramanian, S.N., 2018. Crank angle-resolved exergy analysis of exhaust flows in a diesel engine from the perspective of exhaust waste energy recovery. *Applied Energy*, *216*(C), pp.31-44.

[23] Hawley JG, Wallace FJ, Khalil Arya S. A fully analytical treatment of heat release in diesel engines. J Automobile Eng, Part D, Inst Mech Eng 2003;217 (D8):701–17 (ISSN 0954-4070) Proc Part D, UK; September.

[24] Patankar SV. Numerical heat and mass transfer and fluid flow. Hemisphere Publishing Corporation; 1980.

[25] Dukowicz, J.K., 1980. A particle-fluid numerical model for liquid sprays. *Journal of computational Physics*, *35*(2), pp.229-253.

[26] Beale JC, Reitz RD. (1999). Modeling spray atomization with the Kelvin–Helmholtz/ Rayleigh–Taylor Hybrid Model. Atomization Sprays 9:623–50.

[27] Hanjalić, K., Popovac, M. and Hadžiabdić, M., 2004. A robust near-wall elliptic-relaxation eddy-viscosity turbulence model for CFD. *International Journal of Heat and Fluid Flow*, *25*(6), pp.1047-1051.

[28] Dukowicz JK. Quasi-steady droplet change in the presence of convection. informal report Los Alamos Scientific Laboratory. LA7997-MS.

[29] Liu AB, Reitz RD. (1993). Modeling the effects of drop drag and break-up on fuel sprays. SAE Paper NO. 930072; 1993.

[30] Colin, O., Benkenida, A., 2004. The 3-zones extended coherent flame model (ECFM3Z) for computing premixed/diffusion combustion. Oil Gas Sci. Technol. – Rev. IFP 59 (6), 593–609.

[31] R.W. Haywood. Equilibrium Thermodynamics for Engineers and Scientists. John Wiley & Sons Ltd1980.

[32] A. Bejan. Advanced Engineering Thermodynamics. John Wiley & Sons Canada, Limited1988.

[33] Moran M. J. Availability analysis : a guide to efficient energy use. Englewood Cliffs, N.J. : Prentice-Hall1982.

[34] W.R. Dunbar, N. Lior. Sources of Combustion Irreversibility. Combustion Science and Technology. 103 (1994) 41-61.

[35] C.D. Rakopoulos, E.G. Giakoumis. Second-law analyses applied to internal combustion engines operation. Progress in Energy and Combustion Science. 32 (2006) 2-47.

[36] A.C. Alkidas. The Application of Availability and Energy Balances to a Diesel Engine. Journal of Engineering for Gas Turbines and Power. 110 (1988) 462.

[37] Rakopoulos C.D., Andritsakis E.C. DI and IDI Diesel Engines Combustion Irreversibility Analysis. 1993 American Society of Mechanical Engineers-Winter Annual Meeting, New Orleans, Louisiana, U.S.A., 1993. pp. 17-32

[38] Li, Y., Jia, M., Kokjohn, S.L., Chang, Y. and Reitz, R.D., 2018. Comprehensive analysis of exergy destruction sources in different engine combustion regimes. *Energy*, *149*, pp.697-708.

[39] Rakopoulos, C.D. and Giakoumis, E.G., 2006. Second-law analyses applied to internal combustion engines operation. *Progress in Energy and Combustion science*, *32*(1), pp.2-47.

Table 1

Partitioning of fuel mass between injection pulses

Injection mode	1st pulse mass (kg/cycle)	2nd pulse mass (kg/cycle)
70-30	2.6201×10^{-5}	1.1229×10^{-5}
80-20	2.9944×10^{-5}	0.7486×10^{-5}
90-10	3.3687×10^{-5}	0.3743×10^{-5}

Single injection mass = 3.743×10^{-5} kg/cycle

Table 2

Boundary and initial conditions

Head temperature	550.15 K
Piston temperature	575.15 K
Cylinder temperature	475.15 K
Intake valve closed	52˚CA ATDC
Exhaust valve opening	110˚CA ATDC
Initialized swirl	1500 1/min
Initial TKE	10 m^2/s^2
Initial TDR	5196.15 m^2/s^3

Table 3

Engine specifications

Bore× stroke	82.5× 82 mm
Displacement	438 cm^3/cylinder
Compression ratio	19.5:1
Swirl ratio @ IVC	3
Rail pressure	540-1255 bar (based on engine speed)
Nozzle geometry	5×0.15 mm
Number of nozzles	4
Clearance	0.86mm
Connecting rod length	104mm
Injection start timing	4˚CA BTDC
Residual gas ratio	0.5

Table 4

IMEP values (unit: bar) for different injection modes

Injection mode	10deg	20deg	30deg
70-5-30	5.49	5.64	5.77
70-10-30	5.42	5.452	5.475
70-15-30	5.45	5.448	5.45
70-20-30	5.443	5.43	5.448
80-5-20	5.49	5.58	5.64
80-10-20	5.544	5.519	5.526
80-15-20	5.538	5.539	5.537
80-20-20	5.531	5.531	5.531
90-5-10	5.334	5.36	5.38
90-10-10	5.345	5.3459	5.3467
90-15-10	5.35	5.35	5.3464
90-20-10	5.35	5.3464	5.3464